Smart Soft Actuators and Grippers Enabled by Self-Powered Tribo-Skins

Shoue Chen, Yaokun Pang, Hongyan Yuan, Xiaobo Tan, and Changyong Cao*

Soft end effectors or grippers capable of grasping objects dexterously and efficiently have attracted increasing attention in a broad range of applications. This article describes a smart soft finger-like actuator with fast response, accurate control, self-powered pressure, and bending sensing capability by combing the cable-driven actuation with soft triboelectric nanogenerators (TENGs). The soft actuator, driven by a miniature DC motor, is designed to have multiple segments of elastomer body split with triangular cuts to facilitate the bending actuation and conformal contact with target objects. Two types of TENGs are integrated with the soft actuator: a single-electrode-mode TENG to measure the contact pressure and an inner contact–separation-mode TENG to detect the bending. With micropyramid structures, the tribo-skin patches possess high sensitivity and good compatibility with the actuator and can actively detect proximity, contact, and pressure via self-generated electricity. Based on the modular design approach, a gripper with three fingers is fabricated and tested for its grasping, sensing, and self-powering performance. This gripper is capable of picking up different kinds of objects, providing sensory feedback, and generating electricity, which shows great potential for use in robot–human and robot–environment interaction applications.

1. Introduction

End effectors or grippers are an essential tool integrated with robotic arms for achieving grasping and manipulating functions in a variety of tasks, ranging from picking up and holding objects, to digging and sorting, to locomotion and scratching.[1–3] Inspired by human hands, the majority of traditional robotic grippers are made of assembled rigid joints and links to obtain multiple degrees of freedom (DOFs) for realizing complex gestures or operations.[4] The actuators used for these grippers are installed in the links, joints or gripper base and driven by cables or tendon-like structures.[1,2] A variety of proprioceptive sensors are usually integrated with the grippers, examples of which include tendon tension sensors, torque sensors, encoders, and Hall-effect sensors, to determine the position and velocity of the gripper components, while different kinds of exteroceptive sensors like pressure sensors, electromagnetic sensors and resistive and capacitive sensors are deployed to gather sensory data about the physical properties of the objects.[1] Although these traditional rigid grippers are able to operate accurately and provide a wide range of forces in different kinds of tasks, they are facing challenges in achieving high flexibility and dexterity like human hands, safe interactions with humans and environments, and grasping and manipulating soft or fragile objects.[1,4,5]

Recently, soft grippers have attracted increasing attention from both academia and industry especially for applications involving intensive human–robot or environment–robot interactions.[6] Soft grippers can deform continuously and can safely and gently interact with human and fragile objects without getting damaged. Furthermore, due to their intrinsic softness, such grippers can easily form a conformal contact with objects of sophisticated geometry using a simple control strategy (by exploiting morphological computing), which is a challenge for traditional rigid grippers.[7]

Many different actuation methods have been explored for soft actuators. Examples include pneumatic actuation,[3,8] cable-driven actuation,[9] and actuation based on soft active materials, such as shape memory alloy[10] and electroactive polymers.[11] Pneumatic actuation-based grippers are able to achieve excellent adaptability, good compliance, and large grasping force. However, this method requires additional equipment for supplying air or hydraulic pressure, hindering the dexterity and miniaturization of the whole system.[12] Soft grippers designed based on shape memory alloys tend to have relatively slow response due to the heating and cooling processes, and thus are not suitable for applications demanding fast speed. Although

S. Chen, Dr. Y. Pang, Prof. C. Cao
Laboratory for Soft Machines and Electronics
School of Packaging
Michigan State University
East Lansing, MI 48824, USA
E-mail: ccao@msu.edu
Prof. H. Yuan
Department of Mechanics and Aerospace Engineering
Southern University of Science and Technology
Shenzhen, Guangdong 518055, China
Prof. X. Tan, Prof. C. Cao
Departments of Electrical and Computer Engineering
Mechanical Engineering
Michigan State University
East Lansing, MI 48824, USA

The ORCID identification number(s) for the author(s) of this article can be found under https://doi.org/10.1002/admt.201901075.

**ADVANCED
SCIENCE NEWS**
www.advancedsciencenews.com

**ADVANCED
MATERIALS
TECHNOLOGIES**
www.advmattechnol.de

dielectric elastomer (DEA) shows great promise in developing compact and fast actuators, it requires very high voltages (typically in the range of kilovolts) to produce enough strains or stresses for the actuation, posing safety risks in many applications. On the other hand, cables possess high tensile strength but low or zero bending stiffness (highly flexible), and cable-driven actuation exhibits great advantages in fast speed and simple control.[13] In addition, the actuation force, generated via a motor and applied through the cable, can be delivered along the whole robot's body to a target point (i.e., end effector) to minimize the inertia of the robotic arm and/or gripper.[14] Based on the performance of the motors adopted, cable-driven actuators and grippers have the features of light weight, fast response, and large force output.

To enable the feedback control and probe the environment, various sensors need to be integrated with soft robots, including, in particular, soft grippers. Current strain and pressure sensors employed in the soft robots mainly include resistive sensors,[15] capacitive sensors,[16] piezoelectric sensors,[17] and optical sensors.[18] Although these sensors have been successfully adopted in soft robotics with good performance, they also show some limitations. For example, resistive sensors can measure large strains with high sensitivity and fast response but require an external power source; piezoelectric sensors usually have limited strain ranges; optical sensors are accurate and sensitive in measurements but require rigid cameras. As a result, for a better integration of soft sensors and compliant robotic systems, there is a great need for developing soft sensors possessing high sensitivity, reliability, compliance and flexibility, large measurement range, ease of use and maintenance, and moderate cost. For instance, Li et al. proposed a GelSight Tactile sensor to accurately localize the pose of a part grasped in the robot hand.[19] Xiang et al. developed a TacEA smart end effector by combining a pneumatically actuated visio-tactile sensor and a stretchable electroadhesive pad.[20] Recently, a new kind of soft materials—gallium-based liquid metals (LMs)—is increasingly explored for flexible sensors and actuators in soft robotics due to its high stretchability and electroconductivity.[21] For example, Sheng et al. studied the diverse transformations of LM droplets under controlled electric fields and demonstrated the basic driving principle of planar locomotion of liquid metal objects.[22] Zhang et al. reported that liquid metal droplet can move autonomously by adding some aluminum as fuel, without any assistance of external energy.[23]

Triboelectric nanogenerators (TENGs) based on contact electrification and electrostatic induction have emerged as a promising technology for generating electricity by exploiting mechanical energy such as human body motions.[24,25] The generated electrical voltage by TENGs can also be utilized as a response signal to identify changes in motion or deformation of structures induced by environmental stimuli without the need of an additional power source.[26] Such a self-powered TENG sensor has shown certain desirable advantages, such as low cost, low weight, high sensitivity, excellent versatilities in structural designs, and environment-friendliness. More importantly, thanks to the wide choices for device materials, TENG sensors can have high flexibility and stretchability, making them suitable for flexible and wearable electronics.[27] With these merits,

soft TENG sensors are promising candidates for soft robotics applications.[28]

In this work, we report a smart, cable-driven, finger-like, soft actuator that is capable of fast response, accurate control, and self-powered pressure and bending sensing by combing the cable-driven mechanism with compliant TENG sensors. The bending actuation is driven by a DC motor via a cable. Inspired by human fingers, the soft actuator body is designed to have four segments of elastomer separated by three 45° triangular cuts to facilitate bending and conformal contact with target objects of complex geometries. Two types of TENGs are designed for this soft cable-driven actuator: rubber-based tribo-skin patches (single-electrode mode) attached to the surfaces of phalanges to measure contact pressure, and an inner TENG comprised of two strips (contact–separation mode) located on the backside of the finger to detect bending degrees. The tribo-skin patches are patterned with a micropyramid structure to improve their sensing and harvesting performance. Based on a modular design, an assembled gripper with a three-finger configuration is tested for evaluating its grasping, sensing and energy-harvesting performance.

2. Design and Fabrication of Soft Cable-Driven Actuators

By mimicking human fingers, we propose a novel design for soft smart actuators by integrating soft elastomers, the cable-driven mechanism, and soft TENGs capable of sensing and energy harvesting in bending and contact (tribo-skin for detecting contact pressure and inner TENG strips for measuring curvature) (**Figure 1**a). In this design, the body of the soft actuator is made of silicon rubber and split into four segments by three 45° triangular cuts (the upper segment is inserted into a 3D printed holder for connection), so as to facilitate its bending, and achieve a better enveloping profile and thus a conformal contact with objects of complex geometries. A good enveloping profile in grasping will improve the handling stability and benefit the pressure sensing and energy harvesting for the design of smart actuators. The adjacent phalanx with 45° triangular cuts at its shoulder can provide a 90° angular displacement when bended. The tip phalanx is filleted to resemble a smooth tip-like human finger for grasping. A cable is inserted through the elastomeric body, on the bending side, with one end connected to a miniature DC motor (6 V and 90 rpm, mounted on a 3D-printed holder) through a designed spindle, and the other end fixed on the tip of the finger. In order to protect the body of actuator and reduce potential friction, a plastic tube segment is placed in the hole drilled in each segment. Figure 1b shows the soft cable-driven actuator fabricated according to the dimensions listed in Figure S1 (Supporting Information).

To make the soft actuator smart, we further integrate tribo-skins onto the actuator. The tribo-skin is a rubber-based TENG patch attached to the phalanx surface of the soft actuator, and it can generate electrical energy when the finger contacts external objects. Due to the change of the output voltage with the variation of the contact area under different forces, this TENG can serve as a pressure sensor with high sensitivity after patterning its surface with micropyramid structures. Besides
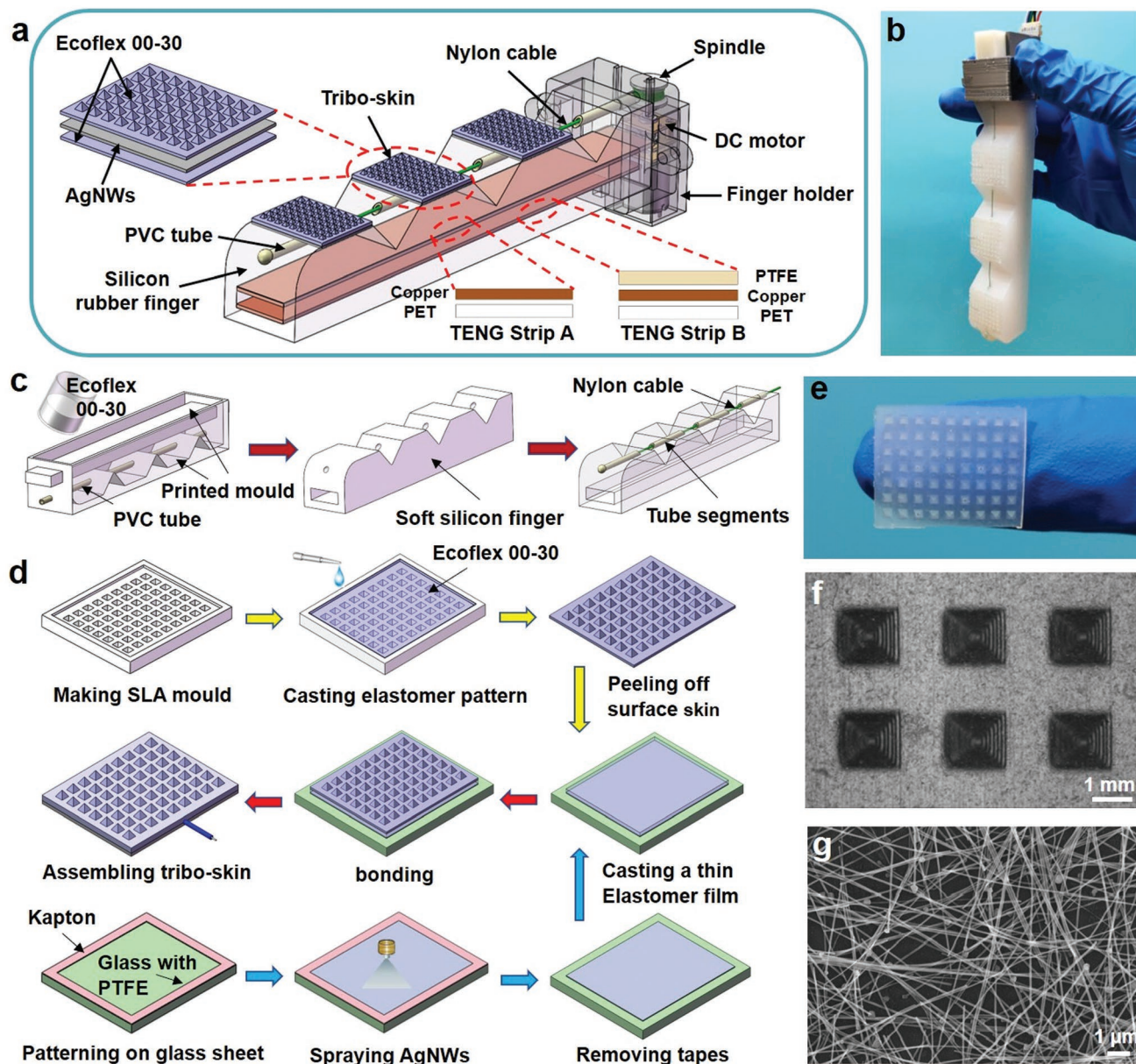
**ADVANCED
SCIENCE NEWS**

www.advancedsciencenews.com

**ADVANCED
MATERIALS
TECHNOLOGIES**

www.advmattechnol.de

Figure 1. Design and fabrication of the intelligent, finger-like, soft actuator with tribo-skins. a) Schematic illustration of the design of a soft cable-driven actuator equipped with tribo-skins and inner TENG strips for energy harvesting and sensing. b) Photograph of the as-fabricated actuator. c) Schematic of the fabrication process for the body of the actuator. d) Schematic of the fabrication process of the tribo-skin patch. e) Photograph of the as-fabricated tribo-skin patch without AgNW electrode deposited. f) Top view (electron microscopy) of the micropyramid structures patterned on the tribo-skin patch for enhancing the performance of TENG (scale bar, 1 mm). g) Scanning electron microscope (SEM) image of the AgNW thin film electrode on the PTFE film (scale bar, 1 µm).

the trio-skins deployed on the surface, another inner TENG designed based on the contact–separate mode is installed along the cavity chamber of the soft actuator (Figure 1a). This inner TENG consists of two separated strips: Strip-A that is connected to the printed holder and Strip-B that is entirely bonded to the inner surface of the chamber along the actuator. When the motor rotates to pull the cable, the soft actuator will bend inward (side with notches) to the degree as specified. When the soft actuator bends, the Strip-A is free from the deformation of the finger due to the boundary condition mentioned above while the Strip-B can curve together with the actuator's

body and thus gets in touch with the Strip-A, resulting in a touched bending of Strip-A. The increased bending of the actuator leads to an increased contact area between the stirps, which in turn produce more electricity thanks to the tribo-electrification effect.[25,29] The output voltage generated by the TENGs can be used to monitor and record the states of the soft actuator in various applications, such as contact force, bending degree, shape profiles and relative weights of contact objects, and in the meantime the harvested electricity energy can also be stored in a capacitor for powering other sensors and electronics as a power source.

Figure 1c shows the fabrication process for the main body of the smart soft actuator. Briefly, a 3D-printed mold, including two separated elements: main stand and space filler, is manufactured by an FDM 3D printer (Zmorph VX) with polylactide (PLA) filament. A Polyvinyl chloride (PVC) plastic tube is inserted into the mold for a coherent hole in the finger actuator to deploy the driven cable. The soft actuator is then mold-casted by pouring the well-mixed Ecoflex 00-30 (Smooth-on Inc., USA) with a weight ratio of 1:1 for parts A and B into the mold. Then, the filled mold is cured at 80 °C for 2 h in an oven. After curing, the space filler and the space tube are removed to demold the soft finger actuator, and then the PVC tube is trimmed into several segments that match the length of the holes in the phalanges. By inserting and bonding the PVC tubes into the holes, the potential friction generated on the elastomer by cable pulling is reduced and thus prevents soft elastomer body from damage. Finally, a Nylon cable is assembled into the soft finger actuator through the tubes with one end tied at the motor spindle and the other fixed on the tip end of the finger actuator. The inner TENG is fabricated by bonding a copper tape onto a polyethylene terephthalate (PET) film with the same size to make Strip-A and then attaching a polytetrafluoroethylene (PTFE) layer at the top of the copper layer bonded with PET film to form Strip-B (Figure S2c, Supporting Information).

The compliant tribo-skin patches are also fabricated using the mold casting method. As shown in Figure 1d, the SLA mold is first printed with a ZRapid Z580 3D printer, and the mold is patterned with an array of micropyramid caves, 1.5 mm (width) × 1.2 mm (height). The as-prepared Ecoflex 00-30 (A:B = 1:1) is mixed by employing a Thinky 300 mixer and poured into the mold for curing at room temperature for 30 min, and the as-made patterned patch is then peeled off from the mold (Figure 1e). After that, a thin electrode is spray-coated onto the patterned patch with AgNW solution (2.5 mg mL^{-1}) to form a tribo-skin. Due to the low adhesion of AgNWs with Ecoflex, we utilize an alternative dry transfer approach to complete this step. In brief, a small glass slide with its surface covered with PTFE film is first prepared for AgNW spraying, then after curing, the AgNW thin film electrode is dry-transferred onto a thin silicon-rubber layer from the glass slide. Finally, the combined tribo-skin with deposited AgNW electrode inside is bonded onto the phalanges via silicon rubber glue (Sil-Poxy). An electric wire will be connected to the AgNW layer for electricity output. Figure 1f shows the top view (via electron microscopy) of the micropyramid structures on the tribo-skin patch, and the AgNWs are uniformly sprayed on the PTFE film and distributed inside the tribo-skin patches (Figure 1g).

3. Sensing and Energy Harvesting Performance of Smart Soft Actuators

3.1. Performance of Inner TENG

The inner TENG with two strips placed in the back section of the actuator works based on the contact–separation mode of triboelectrification effect (**Figure 2**a). The two strips, Strip-A fixed onto the printed holder and Strip-B bonded to the chamber surface, will get into contact when the soft finger-like actuator bends under actuation. Since the two strips have different boundary conditions, Strip-B will deform together with the soft actuator following an equal bending degree. The contact area will increase with further bending of the actuator, making the Strip-A with copper positively charged and Strip-B with PTFE negatively charged according to the triboelectric theory.[30] When the soft finger returns to its original shape, the contacted surfaces separate apart with electrons flowing from Strip-A to Strip-B to neutralize the positive charges triggered by triboelectricity. Electrons keep flowing until the actuator becomes straight. When the actuator is bent again, an inverse electron flow can be generated between the TENG strips. The voltage signal increases with the bending degree of the finger actuator (Figure 2b) and is thus utilized for characterizing the bending profile of the actuator. On the other hand, the measured wavelength of the voltage can be employed to determine the bending frequency of the actuator. Therefore, from this inner TENG sensor, we can quantitively determine the curvature of the soft actuator and the bending profile and speed.

To characterize the performance of the smart soft actuator, we experimentally measure the relationship between the voltage produced by the inner TENG and the bending angles of the soft actuator. Output voltages, currents and transferred charges can be measured by a current preamplifier (Keithley 6514 System Electrometer), and the software LabVIEW is programmed to collect the real-time data in bending process. The motor with an encoder is controlled by Arduino UNO to perform a two-way rotation with specific angular displacements. In the tests, the motor is programmed to rotate to a degree (i.e., 60°, 120°, 180°, ..., 600°) and then rotates back immediately. The generated voltage from the inner TENG is recorded by the Keithley 6514 Electrometer. Figure 2b presents the open-circuit voltage versus the corresponding rotation angles of the motor. With the constant rotation speed of the motor, bending the actuator to a larger degree needs a longer time, which is observed from the increased wave width of the voltage pulse toward the right end of the Figure 2b. Meanwhile, it can be seen that the larger bending degree of the actuator generates higher voltage magnitude, indicating that the voltage signal can be detected and analyzed for reporting the bending degree and bending profile. A peak voltage of 8 V can be obtained from the inner TENG when the soft actuator is bent when the motor rotates by 600°. Based on the shape of the actuator with three phalanges separated by notches and the fact of tip phalanx providing the most supporting forces in the majority of cases, the angle α between the intersection of contour lines of the first and last phalanges of the actuator is selected to describe the motion profile, and use it to relate with the peak value of the voltage induced by the inner TENG (Figure 2c).

The deformation of the soft finger-like actuator is further modeled by finite element method (FEM) with the software package ABAQUS 6.14 (Figure S3, Supporting Information). The four-node tetrahedral element is used to discretize the body of the actuator (Figure S3a, Supporting Information). The Ogden constitutive model is utilized to fit the property of Ecoflex 00-30 with the parameters: $\mu_1 = 0.001887$; $\alpha_1 = -3.848$; $\mu_2 = 0.02225$; $\alpha_2 = 0.663$; $\mu_3 = 0.003574$; $\alpha_3 = 4.225$; $D_1 = 2.93$; $D_2 = 0$; $D_3 = 0$.[31] The top end of the finger is clamped while a displacement loading along vertical direction is applied to the cable
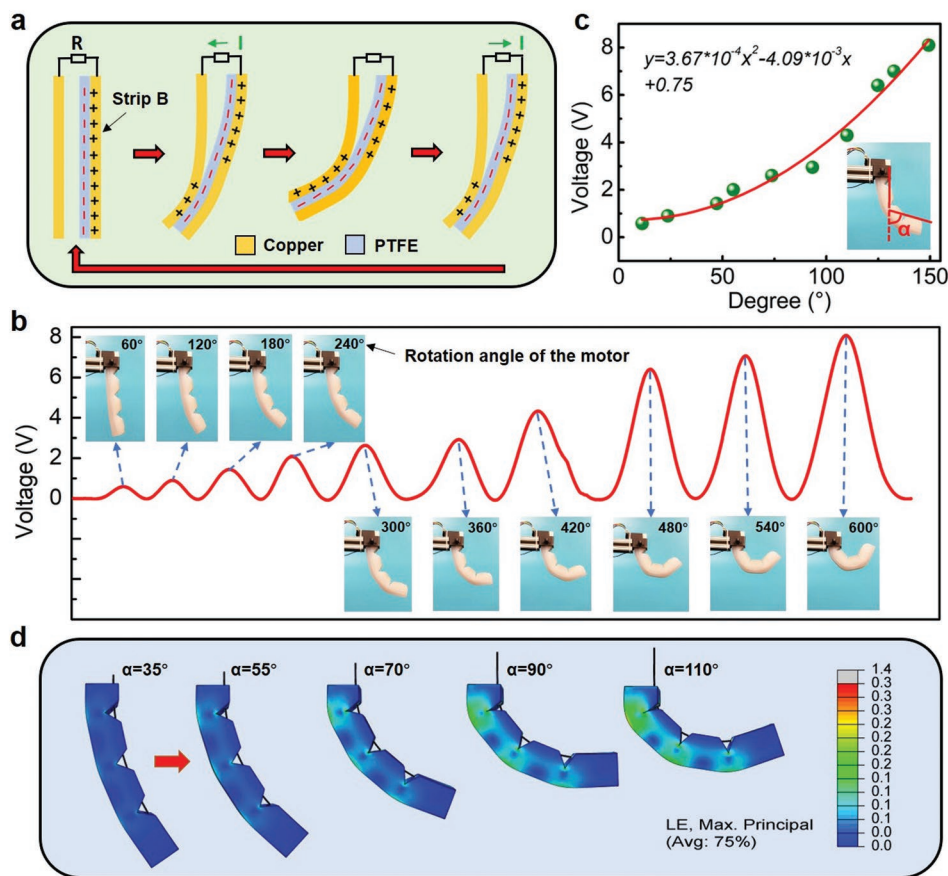
Figure 2. Working mechanism and performance characterization of the inner TENG embedded in the soft actuator. a) Schematic illustration of the working mechanism of the inner TENG: the actuator bends inward to make the inner Strip-B (attached to the finger's chamber) to contact with Strip-A (fixed on the holder) and the contact area increases with the bending degree of the actuator. b) Output voltages generated by the inner TENG for different bending degrees of the soft actuator, measured by the rotation angle of the motor. c) The relationship between the peak voltage induced from the inner TENG and the bending degree of the actuator α (i.e., the intersection angle of contour lines of the first and last phalanxes) and the fitted curve. d) Strain distribution of the cable-driven soft actuator corresponding to some specific bending degrees, obtained by FEM simulation.

to actuate bending. As shown in Figure 2d, when the cable is pulled, the soft actuator gradually bends inward, leading to the notches between the phalanges squeezing together. In addition, the strain distribution of the soft actuator can be simulated to predict the bending profiles of the actuator, as well as the rough grasping force produced by the actuator (Figure 3Sc, Supporting Information).

3.2. Performance of Compliant Tribo-Skin

The soft tribo-skin on each segment is vital for the multifunctionality of this soft actuator, which is capable of sensing contact force and harvesting energy in the actuation operations. To evaluate the performance of energy-harvesting and sensing of the soft tribo-skin under different working conditions, as described in Figure S4 (Supporting Information), we assemble a force gauge with a linear motor (LinMot MBT-37×120). A glass slide is bonded to the tip of a force gauge to allow full-face contact. The linear motor can be precisely adjusted in terms of speed, acceleration and displacement amplitude, and impact the tribo-skin patch periodically. **Figure 3**a describes the

working principle of the tribo-skin patch based on the single-electrode mode.[32] When a dielectric object (i.e., glass slide) approaches the tribo-skin patch, the electrons will be inducted from the ground to the AgNW electrode due to the electrostatic induction effect, inducing electrical currents in the circuit. Charge neutralization occurs and electrons stop moving when the object is in contact with the tribo-skin. When the two surfaces oppositely charged are separated, the potential difference between the AgNW electrode and the ground is induced, prompting the flow of electrons and generating electrical current in the circuit. When the contact object is quite far away from the tribo-skin, a new electrical equilibrium is established.

The tribo-skin can serve as a pressure sensor after the relationship is calibrated between the open-circuit voltage and the amplitude of contact force. Figure 3b–d demonstrates the real-time signals (voltage, current and charge) induced by the as-fabricated tribo-skin under an applied contact force with a magnitude of 8 N and a frequency of 1 Hz. It can be found that the open-circuit voltage achieves a peak value of about 23 V in average, the current induced is about 50–60 nA, and the transferred charge is about 7.5 nC. When the contact force with a frequency of 1 Hz increases from 2 to 10 N with increments
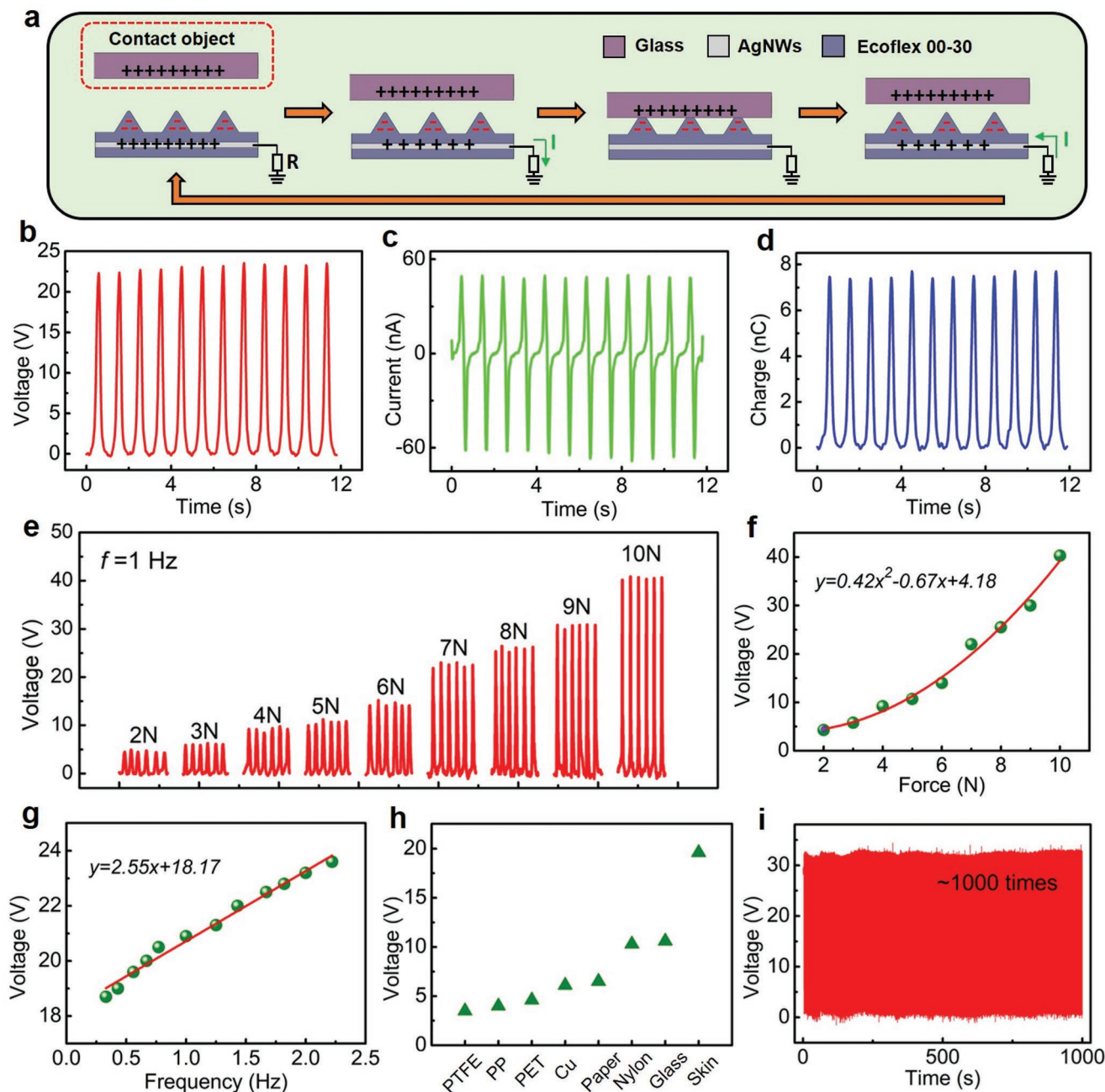
**ADVANCED
SCIENCE NEWS**

www.advancedsciencenews.com

**ADVANCED
MATERIALS
TECHNOLOGIES**

www.advmattechnol.de

Figure 3. Working principle and performance characterization of the tribo-skin patch. a) Schematic illustration of the working mechanism of the soft tribo-skin patch: different contacting area and compression depth are developed based on micropyramid patterns, resulting in pressure-dependent voltage output. b) Open-circuit voltage, c) current, and d) transferred charge generated by the tribo-skin patch under an applied cyclic compression force of 8 N with a frequency of 1 Hz. e) Open-circuit voltages from the tribo-skin patch under different applied forces (1 Hz). f) Fitted curve for the peak voltage by the tribo-skin patch as a function of contact force (1 Hz). g) Effect of the contact frequency on the output voltage of the tribo-skin patch under a force of 7 N. h) Output performance of the tribo-skin affected by the types of object materials. i) Stability and robustness testing of the as-fabricated tribo-skin patch with 1000 contact–separation cycles.

of 1 V, the open-circuit voltage is enhanced from 4.8 to 41 V (Figure 3e). However, further increase in the contact force (>10 N) will not change the output anymore, indicating the sensing limit of this tribo-skin. Figure 3f shows the calibration curve fitted with the data of the peak output voltage and the amplitude of the applied force. Because of the micropyramid

pattern on this tribo-skin patch, the voltage shows nonlinear relationship with the applied contact force, indicating that a smaller force can generate a larger electric output, benefiting its sensing and harvesting capacities.[33]

Contact frequency and contact material are two other factors that influence the electrical outputs of the tribo-skin. Figure 3g
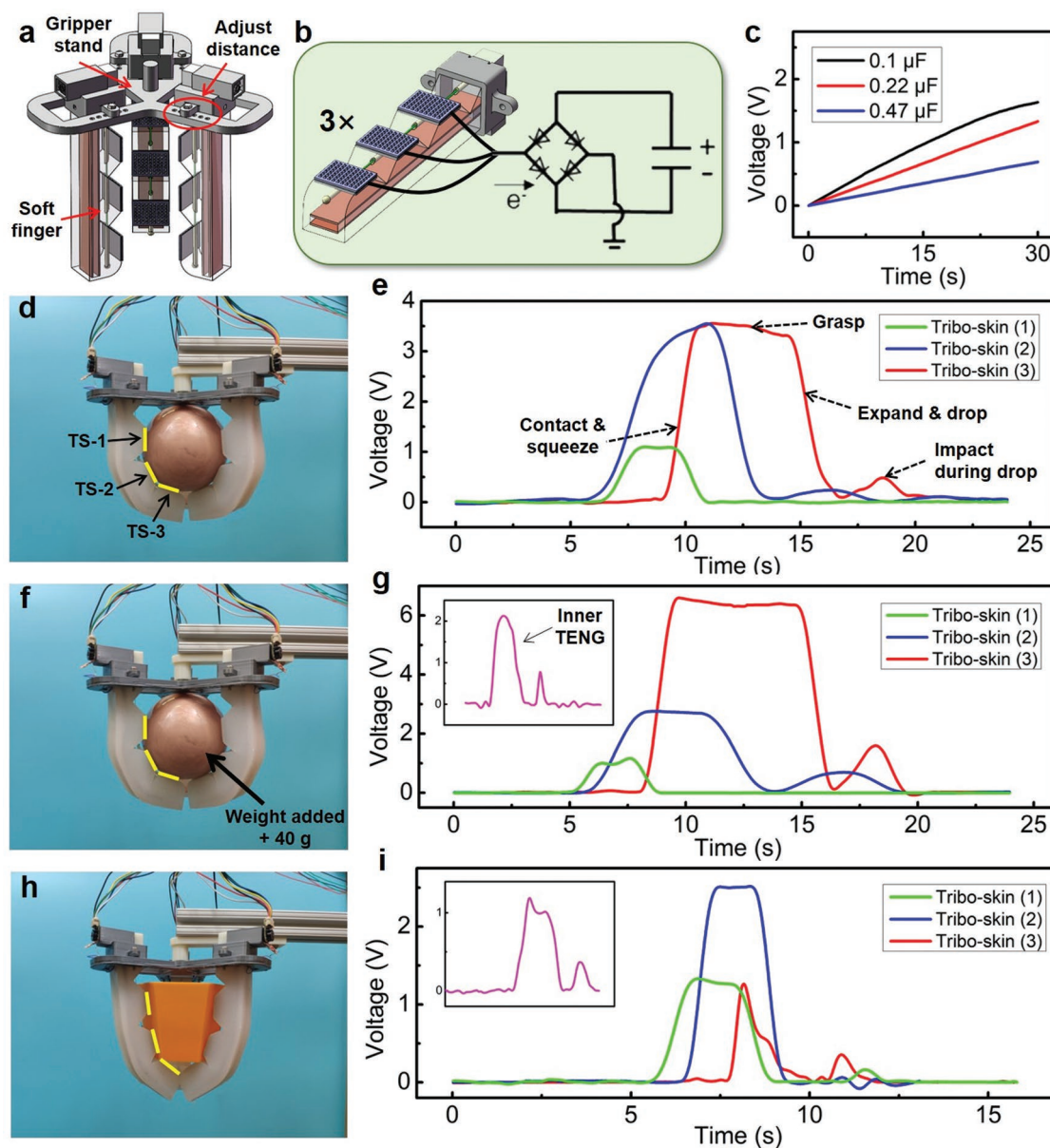
Figure 4. Performance evaluation of a smart soft gripper consisting of three actuators. a) Schematic design of an assembled gripper, in which three finger-like actuators are separated uniformly (120°) and installed on a 3D printed gripper stand. b) Schematic illustration of the electric circuit diagram for the tribo-skin based powering system. c) Charging process of the soft gripper under repetitive grasping/expanding by employing different capacitances. d) Photograph of grasping a plastic ball by the gripper. e) Real-time voltage signals measured from three tribo-skins (TSs) on a single soft actuator, including the contact and squeeze, grasp, expand and drop and secondary impact processes. f) Demonstration of grasping the same object with increased weight. g) Real-time voltage signals from the three tribo-skins along with the voltage from the inner TENG (inset). h) Demonstration of grasping a hexagonal prism. i) Real-time voltage signals from the three tribo-skins along with the voltage from the inner TENG.

shows the peak value of the open-circuit voltage as a function of contact frequency under an applied force of 7 N. It is noticed that the peak voltage is enhanced from 18.7 V to 23.6 V as the frequency increases from 0.3 Hz to 2.2 Hz. As illustrated in Figure 3h, the voltage output produced from tribo-skin varies with the types of object materials. It is observed that under the same amplitude (5 N) and frequency (1 Hz) of the contacts, the human skin, glass and paper are able to generate higher output voltage. Furthermore, we test the robustness and stability of the tribo-skin patch under repeated contact controlled by the linear motor

(1 Hz). It is seen that, within 1000 times of contact–separation cycles in about 16.6 min, the peak value of the open-circuit voltage remains stable (Figure 3i). Therefore, the as-fabricated tribo-skin can serve as a stable force sensor as well as an energy harvester.

4. Performance Evaluation of Soft Smart Grippers

As illustrated in **Figure 4**a, a smart soft gripper can be assembled by three soft finger-like actuators discussed above. Three

**ADVANCED
SCIENCE NEWS**
www.advancedsciencenews.com

**ADVANCED
MATERIALS
TECHNOLOGIES**
www.advmattechnol.de

soft actuators (separated by 120°) are mounted on a 3D-printed stand with threaded holes left there for adjusting grasp scope (grasping diameter ranging from 32 to 82 mm) (Figure 4a). All tribo-skins attached on the fingers of the gripper are connected to a capacitor via a rectifier to store the electricity energy generated during repeated grasping and separating processes (Figure 4b). Through repeated bending of the finger actuator, the voltage of the capacitor (0.1 µF) will gradually increase and reach 1.6 V after 30 s (Figure 4c). The charged capacitor could be further utilized as a power source to drive other sensors or electronics or batteries.

The sensing capability of the gripper is then evaluated by grasping two different objects in the experiment, including an acrylic spherical shell and a polylactic acid (PLA) hexagonal prism. Considering symmetric geometries of the objects, only the voltage signals from the TENG devices (three tribo-skins (TSs) and the inner TENG in one single actuator) need to be monitored. Figure 4d demonstrates the smart gripper can grasp the spherical shell. When the soft fingers bend and approach the spherical ball, TS-2 will first contact with the ball and followed by TS-1, and finally TS-3. The relative position and size of the object with the gripper may affect this contact sequence. The real-time output voltages from tribo-skins (TS-1, TS-2, and TS-3) in a single finger are plotted in Figure 4e. It can be found that TS-1 and TS-2 are the two patches that first get in contact with the ball and TS-3 and TS-2 provide larger forces, reflected by a higher voltage level. When the tribo-skins keep squeezing the object further, the voltage signals will increase to maximum values, and after that, the signals maintain almost constant during grasping and holding. In addition, it is found that when TS-3 contacts the object, TS-1 will no longer provide support force, which is indicated by the vanished voltage. A possible reason is that the last phalanx lifts up the ball and pushes it against the gripper stand, resulting in a gap between the object and the tribo-skin. When the gripper suddenly drops the ball, voltages induced by TS-2 and TS-3 vanish quickly, indicting separations between the object and the tribo-skins. For a heavier object with the same size and shape (Figure 4f), it is observed that the contact sequence of the tribo-skins does not change (Figure 4g). However, the tip phalanx (TS-3) plays a more important role in lifting and grasping this heavier object with its peak output increasing to about 6 V. In addition, the voltage signal produced by TS-2 becomes smaller when grasping and holding the heavier object. Besides these obvious peaks observed in Figure 4e,g, some tiny peaks are also induced from TS-2 and TS-3 after releasing the object, which result from the secondary contact between the object (relatively large size) and the tribo-skins. It is noticed that when the ball falls off, the contact force between the falling object and the TS-3 can produce a voltage peak of 1.6 V (Figure 4g). The real-time voltage from the inner TENG is also plotted as the inset in Figure 4g. When the soft actuator bends to fully grab and hold the ball, the voltage achieves its maximum, approximately 2 V, and the falling of the object will trigger a small signal due to secondary contact as well.

Figure 4h shows a hexagonal prism grasped by the gripper for a short time. Due to the difference in profile, the contact sequence for the tribo-skins becomes TS-1 > TS-2 > TS-3, as shown Figure 4i. In addition, due to the smaller bottom of the prism, TS-3 only touches the bottom edge of this object, thus the voltage signal becomes smaller and sharp during grasping and holding, with a peak voltage of ≈1.2 V. The signal from the inner TENG gives a peak voltage of 1.1 V, and by comparing the bending degrees of the gripper to grasp these two different objects, it is observed that the actuator needs to bend more to wrap the ball, which corresponds to a higher output induced from the inner TENG in Figure 4g. These results prove that the actively generated signals enable the gripper to perceive different actions during grasping an object and to be aware of the dropping and any following contact of the object, indicating their promising use in grasping monitoring and feedback control.

To enable the grasping of heavier objects, we fabricate a soft gripper with stiffer elastomer–Dragon Skin 10 (Smooth-on Inc., USA). **Figure 5** demonstrates its performance in picking and grasping tomatoes for potential agriculture harvesting applications. In this demonstration, because the gripper is fixed on the frame, we hold the stem by hand to pull it down after the gripper grasps the tomato well during the picking operation. It can be seen that as the force needed to pick the tomato off the stem may vary, two samples are prepared before tests. Figure 5b shows the output voltage generated by all the tribo-skins (connected in series) in a single actuator. Different from the voltage presented in Figure 4 for a separate tribo-skin, herein the output voltage gradually increases at the start until the gripper fully holds the tomato. In the picking process, the voltage signal fluctuates obviously, leading to some smaller peaks along the curves. Comparing the two picking up processes, it can be concluded that picking up tomato sample-1 is easier than picking up tomato sample-2, indicated by the smaller voltage and the uniform and tiny peaks along the curves. Therefore, the picking forces can be monitored through the detected voltage signal in the grasping and holding operation during the picking process in agriculture product harvesting.

In the previous demonstration shown in Figure 4, we have shown that the soft gripper can report weight difference by analyzing the voltage signals generated by the tribo-skins. To further verify such a capability in harvesting, we use it to grasp three different tomatoes: 156, 180, and 236 g (Figure 5c). As shown in Figure 5d, the voltage signals of grasping different tomatoes are changed with their weights. Although the slight difference in size may also have affected the voltage profile marginally, voltage signals in the holding stage are mainly influenced by the weight of the tomatoes, which exhibits different levels for different weights. When the soft gripper is grabbing the 156 g tomato, the total voltage induced by three tribo-skins in series at the grasping and holding stage is around 11 V while for grasping a heavier one 180 g, it increases to about 20 V. It is observed that for the heaviest tomato, the output voltage increases to about 35 V. The possible reason is that this weight may be beyond the load capacity of the fabricated gripper which tends to prevent the dropping of such heavy object. For this prototype, the maximum weight it can grasp is around 500 g. Therefore, the proposed soft smart grippers are capable of measuring the contact force and bending degree, and detecting possible secondary contacts, picking force fluctuation and releasing/dropping behaviors. In addition, no matter whether the signal is recorded by separate or combined tribo-skins, it can be successfully utilized to identify the weight/mass difference.
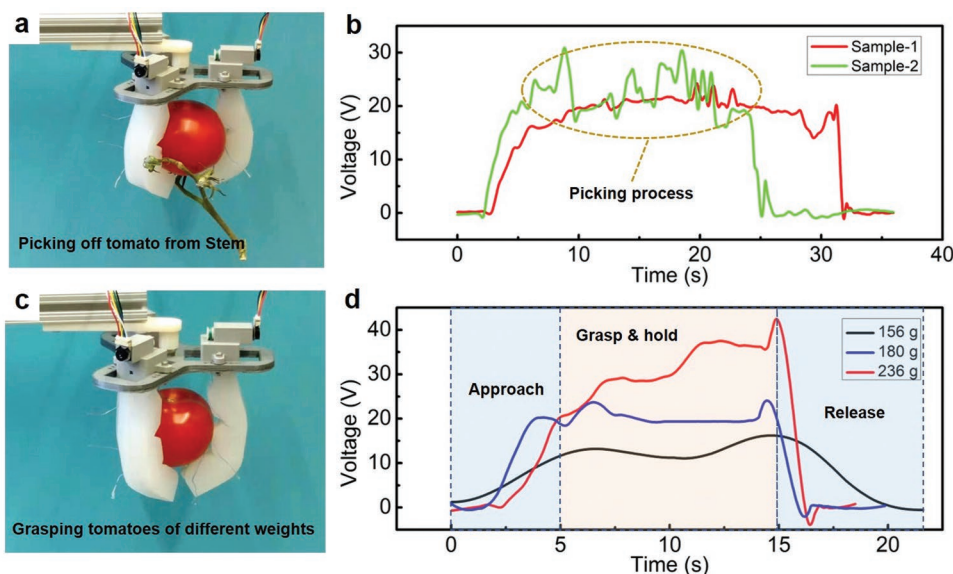
Figure 5. Demonstration and testing of picking off tomatoes by using a smart soft gripper. a) Photograph of picking off tomatoes from its stem. b) Measured real-time voltage signals by all three tribo-skins (in series) on the gripper in the picking process, including the approach, grasp and holding, and release process. c) Photograph of grasping tomatoes with different weights. d) Measured real-time voltage signals generated by all tribo-skins on the gripper when the gripper grasping tomatoes with different weights, including the approach, grasp and holding, and release process.

5. Conclusion

In summary, we have proposed a smart soft actuator with self-powered sensing tribo-skins through the integration of soft elastomers, cable-driven mechanism and TENGs. Two different types of TENGs are equipped in the soft cable-driven actuators: the inner TENG based on the contact–separation mode that is able to generate voltage signals reflecting the bending degree of the actuator, and the tribo-skin patches that are patterned with micropyramids on surface and AgNW stretchable electrode that can sense contact pressure while harvesting energy through the single mode TENG design. The TENG-based sensors can be employed for monitoring the contact forces on objects, bending angles of the finger actuator and even relative weight and rough profile of the touched objects. However, it is noted that the electrical output by the inner TENG is not very competitive for energy harvesting due to its relatively grasping frequency in many practical applications.

This finger-like actuator can be further assembled together with a modular design strategy to form smart grippers for diverse applications. The experiments have demonstrated that a three-fingered gripper can be used to complete different kinds of tasks, and perceive different motions including approaching, grabbing, releasing, paving the way for building highly efficient but simple robotic hands for broad applications. However, it is observed that the sensing performance of the tribo-skin is strongly affected by other factors, including the materials of contact objects, humidity and temperature. In addition, the contact area of the tribo-skin may vary from partial to full surface in grasping due to the shape variation of grasped objects, which will be challenging for calibration. Thus, to get a reliable detection behavior, other factors should be kept constant during operation, which is not a problem in factory but would be challenging in outer spaces.

One solution is to design the TENG-based skin with the contact–separation mode, which can get rid of the influences from contact materials and other environmental factors like humidity. Furthermore, with integration with techniques such as machine learning, the gripper may be able to identify different features (shape, hardness, etc.) of the grasped objects.

Supporting Information

Supporting Information is available from the Wiley Online Library or from the author.

Conflict of Interest

The authors declare no conflict of interest.

Keywords

artificial skins, cable-driven actuators, soft grippers, soft sensors, triboelectric nanogenerators

[1] J. Shintake, V. Cacucciolo, D. Floreano, H. Shea, *Adv. Mater.* **2018**, *30*, 1707035.

[2] J. Hughes, U. Culha, F. Giardina, F. Guenther, A. Rosendo, F. Iida, *Front. Robo. AI* **2016**, *3*, 69.

[3] M. Manti, T. Hassan, G. Passetti, N. D'Elia, C. Laschi, M. Cianchetti, *Soft Rob.* **2015**, *2*, 107.

[4] R. Balasubramanian, V. J. Santos, *The Human Hand as an Inspiration for Robot Hand Development*, Vol. 95, Springer International Publishing, Cham, Switzerland **2014**.

[5] M. G. Catalano, G. Grioli, E. Farnioli, A. Serio, C. Piazza, A. Bicchi, *Int. J. Rob. Res.* **2014**, *33*, 768.

[6] C. Laschi, M. Cianchetti, *Front. Bioeng. Biotechnol.* **2014**, *2*, 3.

[7] J. Hughes, U. Culha, F. Giardina, F. Guenther, A. Rosendo, F. Iida, *Front. Robot. AI* **2016**, *3*, 69.

[8] a) Y. Hao, Z. Gong, Z. Xie, S. Guan, X. Yang, Z. Ren, T. Wang, L. Wen, presented at *2016 35th Chinese Control Conference (CCC)*, Chengdu, China, July **2016**; b) B. Mosadegh, P. Polygerinos, C. Keplinger, S. Wennstedt, R. F. Shepherd, U. Gupta, J. Shim, K. Bertoldi, C. J. Walsh, G. M. Whitesides, *Adv. Funct. Mater.* **2014**, *24*, 2163.

[9] a) T. Hassan, M. Manti, G. Passetti, N. d'Elia, M. Cianchetti, C. Laschi, in *Conf. Proc.: Annu. Int. Conf. of the IEEE Engineering in Medicine and Biology Society*, IEEE, Piscataway, NJ **2015**, p. 3619; b) V. Slesarenko, S. Engelkemier, P. I. Galich, D. Vladimirsky, G. Klein, S. Rudykh, *Polymers* **2018**, *10*, 846.

[10] a) S. Yan, X. Liu, F. Xu, J. Wang, *J. Intell. Mater. Syst. Struct.* **2007**, *18*, 459; b) K. Yang, Y. Wang, *J. Mech. Sci. Technol.* **2008**, *22*, 895; c) Z. Zhong, C. Yeong, *Sens. Actuators, A* **2006**, *126*, 375.

[11] a) S. Shian, K. Bertoldi, D. R. Clarke, *Adv. Mater.* **2015**, *27*, 6814; b) O. A. Araromi, I. Gavrilovich, J. Shintake, S. Rosset, M. Richard, V. Gass, H. R. Shea, *Appl. Phys. Lett.* **2017**, *110*, 182906; c) G.-K. Lau, K.-R. Heng, A. S. Ahmed, M. Shrestha, *Appl. Phys. Lett.* **2017**, *110*, 182906.

[12] B. Verrelst, R. Van Ham, B. Vanderborght, D. Lefeber, F. Daerden, M. Van Damme, *Adv. Rob.* **2006**, *20*, 783.

[13] M. Calisti, M. Giorelli, G. Levy, B. Mazzolai, B. Hochner, C. Laschi, P. Dario, *Bioinspiration Biomimetics* **2011**, *6*, 036002.

[14] D. B. Camarillo, C. F. Milne, C. R. Carlson, M. R. Zinn, J. K. Salisbury, *IEEE Trans. Rob.* **2008**, *24*, 1262.

[15] a) C. L. Choong, M. B. Shim, B. S. Lee, S. Jeon, D. S. Ko, T. H. Kang, J. Bae, S. H. Lee, K. E. Byun, J. Im, *Adv. Mater.* **2014**, *26*, 3451; b) L. Pan, A. Chortos, G. Yu, Y. Wang, S. Isaacson, R. Allen, Y. Shi, R. Dauskardt, Z. Bao, *Nat. Commun.* **2014**, *5*, 3002; c) B. Zhu, Z. Niu, H. Wang, W. R. Leow, H. Wang, Y. Li, L. Zheng, J. Wei, F. Huo, X. Chen, *Small* **2014**, *10*, 3625.

[16] a) A. Frutiger, J. T. Muth, D. M. Vogt, Y. Mengüç, A. Campo, A. D. Valentine, C. J. Walsh, J. A. Lewis, *Adv. Mater.* **2015**, *27*, 2440; b) G. Schwartz, B. C.-K. Tee, J. Mei, A. L. Appleton, D. H. Kim, H. Wang, Z. Bao, *Nat. Commun.* **2013**, *4*, 1859; c) S. C. Mannsfeld, B. C. Tee, R. M. Stoltenberg, C. V. H. Chen, S. Barman, B. V. Muir, A. N. Sokolov, C. Reese, Z. Bao, *Nat. Mater.* **2010**, *9*, 859.

[17] a) H. Gullapalli, V. S. Vemuru, A. Kumar, A. Botello-Mendez, R. Vajtai, M. Terrones, S. Nagarajaiah, P. M. Ajayan, *Small* **2010**, *6*, 1641; b) D. Mandal, S. Yoon, K. J. Kim, *Macromol. Rapid Commun.*

[18] a) B. Winstone, G. Griffiths, T. Pipe, C. Melhuish, J. Rossiter, in *Conf. on Biomimetic and Biohybrid Systems* (Eds: N. F. Lepora, A. Mura, H. G. Krapp, P. F. M. J. Verschure, T. J. Prescott), Springer, Berlin **2013**; b) S. Yun, S. Park, B. Park, Y. Kim, S. K. Park, S. Nam, K. U. Kyung, *Adv. Mater.* **2014**, *26*, 4474; c) Y.-L. Park, K. Chau, R. J. Black, M. R. Cutkosky, presented at *Proc. 2007 IEEE Int. Conf. on Robotics and Automation*, Roma, Italy, April **2007**.

[19] R. Li, R. Platt, W. Yuan, A. ten Pas, N. Roscup, M. A. Srinivasan, E. Adelson, presented at *2014 IEEE/RSJ Int. Conf. on Intelligent Robots and Systems*, Chicago, IL, September **2014**.

[20] C. Xiang, J. Guo, J. Rossiter, *Smart Mater. Struct.* **2019**, *28*, 055034.

[21] A. Ahmed, S. L. Zhang, I. Hassan, Z. Saadatnia, Y. Zi, J. Zu, Z. L. Wang, *Extreme Mech. Lett.* **2017**, *13*, 25.

[22] L. Sheng, J. Zhang, J. Liu, *Adv. Mater.* **2014**, *26*, 6036.

[23] J. Zhang, Y. Yao, L. Sheng, J. Liu, *Adv. Mater.* **2015**, *27*, 2648.

[24] a) F.-R. Fan, Z.-Q. Tian, Z. Lin Wang, *Nano Energy* **2012**, *1*, 328; b) Z. L. Wang, *ACS Nano* **2013**, *7*, 9533; c) S. Niu, X. Wang, F. Yi, Y. S. Zhou, Z. L. Wang, *Nat. Commun.* **2015**, *6*, 8975; d) Y. Pang, S. Chen, Y. Chu, Z. L. Wang, C. Cao, *Nano Energy* **2019**, *66*, 104131; e) H. Yang, Y. Pang, T. Bu, W. Liu, J. Luo, D. Jiang, C. Zhang, Z. L. Wang, *Nat. Commun.* **2019**, *10*, 2309; f) F. Xi, Y. Pang, G. Liu, S. Wang, W. Li, C. Zhang, Z. L. Wang, *Nano Energy* **2019**, *61*, 1.

[25] C. Zhang, W. Tang, C. Han, F. Fan, Z. L. Wang, *Adv. Mater.* **2014**, *26*, 3580.

[26] a) S. Wang, L. Lin, Z. L. Wang, *Nano Energy* **2015**, *11*, 436; b) J. Luo, W. Tang, F. R. Fan, C. Liu, Y. Pang, G. Cao, Z. L. Wang, *ACS Nano* **2016**, *10*, 8078; c) Y. K. Pang, X. H. Li, M. X. Chen, C. B. Han, C. Zhang, Z. L. Wang, *ACS Appl. Mater. Interfaces* **2015**, *7*, 19076.

[27] a) K. Dong, X. Peng, Z. L. Wang, *Adv. Mater.* **2019**, 1902549, https://doi.org/10.1002/adma.201902549; b) Q. Jiang, C. Wu, Z. Wang, A. C. Wang, J.-H. He, Z. L. Wang, H. N. Alshareef, *Nano Energy* **2018**, *45*, 266; c) Y. Pang, J. Li, T. Zhou, Z. Yang, J. Luo, L. Zhang, G. Dong, C. Zhang, Z. L. Wang, *Nano Energy* **2017**, *31*, 533.

[28] a) Y. C. Lai, J. Deng, R. Liu, Y. C. Hsiao, S. L. Zhang, W. Peng, H. M. Wu, X. Wang, Z. L. Wang, *Adv. Mater.* **2018**, *30*, 1801114; b) J. Chen, B. Chen, K. Han, W. Tang, Z. L. Wang, *Adv. Mater. Technol.* **2019**, *4*, 1900337; c) X. Pu, H. Guo, Q. Tang, J. Chen, L. Feng, G. Liu, X. Wang, Y. Xi, C. Hu, Z. L. Wang, *Nano Energy* **2018**, *54*, 453; d) Y. Xi, H. Guo, Y. Zi, X. Li, J. Wang, J. Deng, S. Li, C. Hu, X. Cao, Z. L. Wang, *Adv. Energy Mater.* **2017**, *7*, 1602397.

[29] Z. L. Wang, J. Chen, L. Lin, *Energy Environ. Sci.* **2015**, *8*, 2250.

[30] A. Yu, Y. Zhu, W. Wang, J. Zhai, *Adv. Funct. Mater.* *29*, **2019**, 1900098.

[31] G. Agarwal, N. Besuchet, B. Audergon, J. Paik, *Sci. Rep.* **2016**, *6*, 34224.

[32] a) G. Zhu, W. Q. Yang, T. Zhang, Q. Jing, J. Chen, Y. S. Zhou, P. Bai, Z. L. Wang, *Nano Lett.* **2014**, *14*, 3208; b) S. Niu, Y. Liu, S. Wang, L. Lin, Y. S. Zhou, Y. Hu, Z. L. Wang, *Adv. Funct. Mater.* **2014**, *24*, 3332; c) S. W. Chen, X. Cao, N. Wang, L. Ma, H. R. Zhu, M. Willander, Y. Jie, Z. L. Wang, *Adv. Energy Mater.* **2017**, *7*, 1601255.

[33] F.-R. Fan, L. Lin, G. Zhu, W. Wu, R. Zhang, Z. L. Wang, *Nano Lett.* **2012**, *12*, 3109.